Journal of Biomedical Optics

BiomedicalOptics.SPIEDigitalLibrary.org

Optical coherence elastography of cold cataract in porcine lens

Hongqiu Zhang
Chen Wu
Manmohan Singh
Achuth Nair
Salavat R. Aglyamov
Kirill V. Larin

SPIE.

Hongqiu Zhang, Chen Wu, Manmohan Singh, Achuth Nair, Salavat R. Aglyamov, Kirill V. Larin, "Optical coherence elastography of cold cataract in porcine lens," *J. Biomed. Opt.* **24**(3), 036004 (2019), doi: 10.1117/1.JBO.24.3.036004.

Optical coherence elastography of cold cataract in porcine lens

Hongqiu Zhang,[a] Chen Wu,[a] Manmohan Singh,[a] Achuth Nair,[a] Salavat R. Aglyamov,[b,c] and Kirill V. Larin[a,*]
[a]University of Houston, Department of Biomedical Engineering, Houston, Texas, United States
[b]University of Houston, Department of Mechanical Engineering, Houston, Texas, United States
[c]University of Texas at Austin, Department of Biomedical Engineering, Austin, Texas, United States

Abstract. Cataract is one of the most prevalent causes of blindness around the world. Understanding the mechanisms of cataract development and progression is important for clinical diagnosis and treatment. Cold cataract has proven to be a robust model for cataract formation that can be easily controlled in the laboratory. There is evidence that the biomechanical properties of the lens can be significantly changed by cataract. Therefore, early detection of cataract, as well as evaluation of therapies, could be guided by characterization of lenticular biomechanical properties. In this work, we utilized optical coherence elastography (OCE) to monitor the changes in biomechanical properties of *ex vivo* porcine lenses during formation of cold cataract. Elastic waves were induced in the porcine lenses by a focused micro air-pulse while the lenses were cooled, and the elastic wave velocity was translated to Young's modulus of the lens. The results show an increase in the stiffness of the lens due to formation of the cold cataract (from 11.3 ± 3.4 to 21.8 ± 7.8 kPa). These results show a relation between lens opacity and stiffness and demonstrate that OCE can assess lenticular biomechanical properties and may be useful for detecting and potentially characterizing cataracts. [DOI: 10.1117/1.JBO.24.3.036004]

Keywords: optical coherence elastography; cold cataract; crystalline lens; tissue biomechanical properties.

Paper 180649R received Dec. 5, 2018; accepted for publication Feb. 19, 2019; published online Mar. 12, 2019.

1 Introduction

Cataract is clouding of the crystalline lens that can severely impair vision with faded colors, blurry vision, halos around light, and poor night vision. Approximately one-third of all people with some form of vision impairment have cataract.[1] Eventually, over half of patients with cataract undergo vision loss.[1] There are numerous causes of cataract, such as aging, trauma, diabetes, obesity, congenital genetic deficiencies, and environmental exposure to toxins.[2] Usually, cataract is progressive and requires surgical interventions for treatment. The specific underlying mechanism of cataract formation is still unknown, but there are reports that the stiffness of the cataract lenses in humans is significantly higher than that of normal lenses.[3]

One of the simplest models to investigate cataract formation is a cold cataract. Cold cataract is a reversible opacification induced in the nucleus of lenses by lowering the temperature.[4,5] This phenomenon enables us to study a controlled opacification and to investigate the physicochemical processes associated with a reversible form of cataract. It has been shown that the precipitation of γ-crystallin is correlated with cold cataract development in the lens.[6] Gamma crystallin is one of the predominant crystallins in the lens nucleus that is responsible for optical transparency.[4] This reversible opacification is a result of a phase separation of the cytoplasmic proteins into coexisting protein-rich and protein-poor liquid domains. Zigman and Lerman[5] demonstrated that γ-crystallin is the major component of both fractions. Gamma crystallin has been shown to be the only one of the three soluble protein fractions capable of acting as a cryoprotein. The relative concentration of γ-crystallin as compared with the amounts of α- or β-crystallin in solution determines whether cold precipitation occurs. Therefore, since the nucleus of the lens contains more γ-crystallin than the cortex, opacification predominantly occurs in the lens nucleus.[4] Moreover, the concentration of γ-crystallin can also affect the appearance of cold cataract.[6] Previous research has been focused on biomolecular and biochemical changes during cold cataract formation.[7–9] For example, the formation of cold cataract has been observed in lenses of various animals, such as fish and cattle, and the contribution of different types of crystallins was evaluated.[8,9] Moreover, the optical characteristics of lenses with cold cataract were assessed.[7,10] Despite this research, there is a lack of work focused on the biomechanical effects of cold cataract on the lens.

Mechanical testing is commonly used to evaluate the biomechanics of ocular tissue, including the lens; however, these techniques are invasive and destructive, which limits their clinical applicability.[11,12] Several nondestructive techniques have been proposed to evaluate lenticular biomechanical properties,[13–15] including acoustic-based elastographic techniques.[13,16–18] While these techniques have revealed critical information, they lack spatial resolution and sufficient contrast.

Optical coherence tomography (OCT) is capable of noninvasive depth-resolved imaging with micrometer-scale resolution up to ~2 mm in scattering media such as tissue.[19,20] Optical coherence elastography (OCE), the elastographic functional extension of OCT, takes advantage of the high resolution and high sensitivity capabilities of OCT and has subnanometer displacement sensitivity with phase-resolved detection.[21–23] The high resolution, large dynamic range, superior contrast, high displacement sensitivity, and noninvasive imaging of OCE make it an effective tool for evaluating the biomechanical

*Address all correspondence to Kirill V. Larin, E-mail: klarin@uh.edu

properties of small, thin tissues, such as those in the eye.[21,24] In our previous work, we have used dynamic OCE and acoustic-based methods for noninvasively assessing lenticular biomechanical properties.[25–29] We have demonstrated that the biomechanical properties of the crystalline lens can be measured *in situ* and quantified variations in the stiffness of mammalian lenses as a function of age and intraocular pressure.[25,27–29] Shear wave elastography is one of the most common elastography techniques because it does not need *a priori* information about the sample or excitation, and it can be performed completely noninvasively.[30] Ultrasound-based shear wave elastography techniques have been used to evaluate the biomechanical properties of various animal lenses.[25,31,32] However, the low resolution, poor contrast, and large excitation forces of ultrasound-based techniques may not be suitable for *in vivo* applications. Thus, we propose the use of OCE to detect elastic waves in the lens to characterize lenticular biomechanical properties.

In this work, we induced cold cataracts in *ex vivo* porcine lenses and assessed the lenticular stiffness with elastic wave-based OCE. After OCE measurements of the fresh lenses during temperature decrease, the cold cataract was induced by lowering the temperature of the isolated crystalline lenses for 6 h. Then, the OCE measurements were repeated as the temperature was increased. After the cataract formation, the lenses showed an increase in elastic wave velocity in comparison with fresh lenses. The difference in wave velocity between cataract and fresh lenses disappeared after the cataract dissolved. The results indicate the stiffness of the lens has a correlation with lens opacity in a cold cataract model.

2 Materials and Methods

The OCE system was based on a home-built spectral domain OCT (SD-OCT) system and an air-pulse excitation system, as shown in Fig. 1.[33,34] The SD-OCT system utilized a superluminescent diode light source with a central wavelength of 840 nm, bandwidth of 49 nm, and output power of 18 mW. The acquisition speed of the camera was set as 25 kHz. The displacement sensitivity of the OCE system was measured as 12 nm in air. The air-pulse delivery system used an electronically controlled pneumatic solenoid and control unit to produce a short duration air-pulse (<1 ms) that was synchronized with the SD-OCT system frame trigger.[35] To image deep inside the lens and visualize the formation of the cold cataract, we utilized a commercial swept source OCT (SS-OCT) system (OCS1310V2, Thorlabs Inc., New Jersey) with a central wavelength of 1300 nm, bandwidth of ~100 nm, and sweep rate of 200 kHz.[36]

Preliminary measurements were performed on tissue-mimicking agar phantoms (1%, w/w, Difco Nutrient Agar from BD, Franklin Lakes, New Jersey) and gelatin phantoms (3%, w/w, Type A gelatin, 250 Bloom/8 Mesh, PB Gelatins/PB Leiner, Davenport, Iowa). The phantoms were cast by standard methods as described in our previous work.[34,37] Cylindrical culture dishes with inner diameter of 50 mm and height of 12 mm were used to mold the phantom samples. After that, the samples were placed into the refrigerator at ~4°C.[37] The phantoms were measured by OCE as the phantoms warmed ($N = 3$ for both gelatin and agar phantoms). The phantom temperature was controlled by the system consisting of a holder and a thermoelectric cooler that was used also to control the temperature of the lenses shown in Fig. 1. In addition, the temperature on the phantom surface was monitored by a noncontact infrared thermometer (CF-IR, ThermoWorks, Utah).

Seven whole porcine eyes from animals within 4 to 6 months of age were shipped overnight on ice (Sioux-Preme Packing Co., Iowa). The freshly extracted lenses were placed in the custom apparatus of the temperature controlling system. The lenses were half submerged in 1× phosphate buffered saline (PBS) when OCE measurements were not being performed. Additional 1× PBS was topically dropped on to the upper surface of the lenses every 20 s to make sure the lenses were hydrated. Measurements of the fresh lenses were taken at 3°C intervals from 21°C to 6°C. It required ~5 min to reach the 3°C temperature increase for every step. Once the target temperature was reached, we waited for 2 min to make sure the temperature of the thermoelectric cooler was the same as that of the noncontact thermometer. After the initial measurements on the fresh lenses, the lenses were put into a 4°C refrigerator for 6 h, also submerged in 1× PBS, to induce a cold cataract. Cold cataract was identified by visual inspection and confirmed by SS-OCT imaging. The lenses were removed from the refrigerator, placed in a holder, and the OCT imaging and OCE measurements were repeated for the chilled lenses while temperature was increased from 6°C to 21°C, also at 3°C increments with the same measurement interval.

To evaluate the temperature distribution inside the samples, separate experiments were performed on a 1% agar phantom and porcine lens. The samples were partially immersed in the PBS solution as with the previous measurements. A thermocouple (Omega Engineering Inc., Norwalk, Connecticut) with a diameter of 0.1 mm was used to probe the temperature gradient

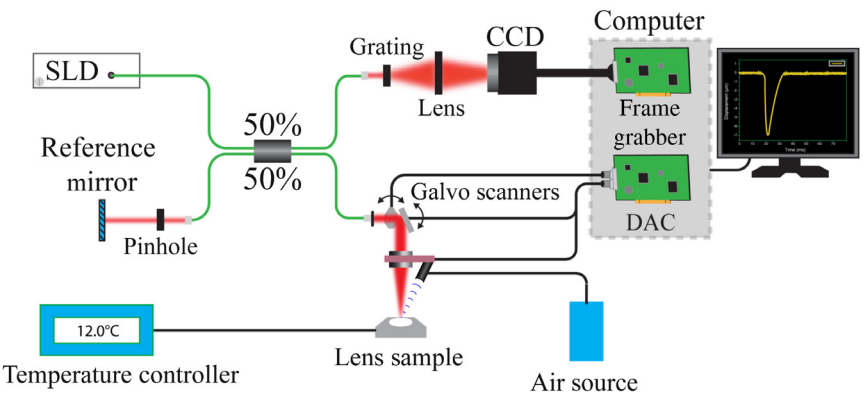

Fig. 1 Schematic of the experimental setup during the OCE measurements.

inside the samples at four equally spaced positions along the entire depth of the sample 2 min after the temperature reading from the temperature control system was stable.

OCE measurements were performed by inducing small amplitude displacements ($\leq 10\ \mu$m) using a short duration air-pulse ($\leq$1 ms) on the surface of the lenses and phantoms. M-B-mode imaging was performed, where the OCT probe beam was held stationary at a given position, and an air-pulse was excited by the air-pulse system. Then, the OCT probe beam was moved to the next position and another elastic wave was excited. By synchronizing the OCT system frame trigger with the air-pulse control unit, we effectively imaged the same elastic wave at a frame rate equal to the OCT system A-scan rate (i.e., camera speed).[35] Successive M-mode images ($n = 251$) were acquired by the SD-OCT system over a ~6.1 mm line, where the center of the scan and air-pulse excitation were at the apex of the lens. The scan time for one position was ~10 ms, and the entire M-B scan time was ~30 s. The air-pulse induced a low-amplitude displacement at the apex of the lens, which then propagated transversely as an elastic wave. The raw temporal phase profiles were unwrapped and then converted to displacement after correcting for the refractive index mismatch and surface motion.[38] The displacement profiles along the propagation path (i.e., along the curvature of the sample) were then processed by a cross-correlation algorithm to obtain the elastic wave propagation delays. In short, the displacement profile at the excitation was used as a reference profile, and the displacement profiles from successively more distant positions were then cross-correlated with the reference profile. The peak of the subsequent cross-correlation was selected as the temporal delay for the elastic wave propagation to that OCE measurement position. A linear fit was then performed on the elastic wave propagation delays and their corresponding distances (incorporating the curvature of the sample). We selected the ~3 mm central part of the lens for the group velocity estimation to make sure that the measured group velocity was over cold cataract. The speed of the elastic wave was converted to the Young's modulus value (E) by the surface wave equation [39,40]

$$E = \frac{2\rho(1+v)^3}{(0.87+1.12v)^2}c_g^2, \tag{1}$$

where $\rho = 1183\ \text{kg/m}^3$ was the lens density,[41] $v = 0.5$ was Poisson's ratio,[42] and c_g was the OCE-measured elastic wave group velocity. Before testing, all porcine lenses were physically measured, and there were no detectable changes in sample geometry.

3 Results

Figure 2 shows the OCE-measured group velocities for agar and gelatin phantoms as a function of temperature. As seen in Fig. 2, gelatin and agar gels demonstrate different levels of dependence of the elastic wave speed on temperature. While the group velocity in the gelatin phantom decreased from ~1.9 to ~1.7 m/s as the temperature increased from 5°C to 20°C, the velocity in the agar phantom did not show significant changes with temperature, decreasing from 2.2 to 2.1 m/s. Statistical testing by a one-way ANOVA showed that there was statistical significance of samples on the stiffness of the 3% gelatin phantoms $[F(2, 0.95) = 5.00,\ p = 0.03]$ but no statistical significance of samples on the stiffness of the 1% agar phantoms $[F(2, 0.95) = 2.46,\ p = 0.14]$ as a function of temperature.

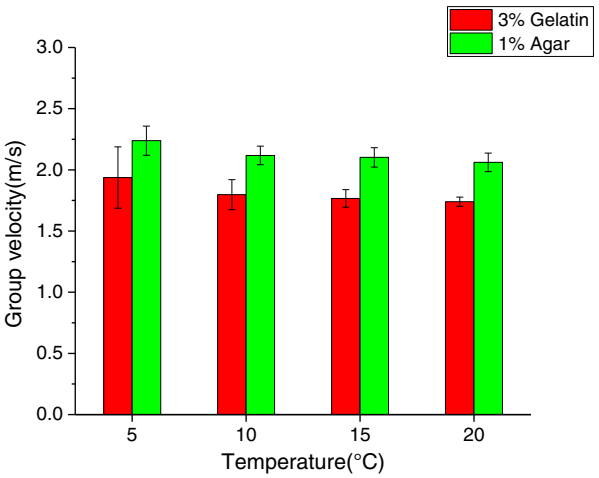

Fig. 2 The OCE-measured group velocity in a 3% gelatin and 1% agar phantoms as a function of temperature.

Additional measurements of the temperature gradient in the agar phantom demonstrated a monotonic dependence of the temperature with depth, such that the maximum difference between the top of the phantom exposed to air and PBS solution was 1.5°C. The mean difference between the temperature inside the phantom and PBS solution was 0.55°C with a standard deviation of 0.56°C.

Figure 3 shows images taken by a standard dissecting microscope (Stemi 508, Carl Zeiss Microscopy, LLC, Thornwood, New York) while (a) chilling the fresh lens from 21°C to 6°C and (b) warming the lens from 6°C to 21°C after being placed in a 4°C refrigerator for 6 h. As seen in Fig. 3(a), the fresh lens was clear, and there was no apparent change in the lens

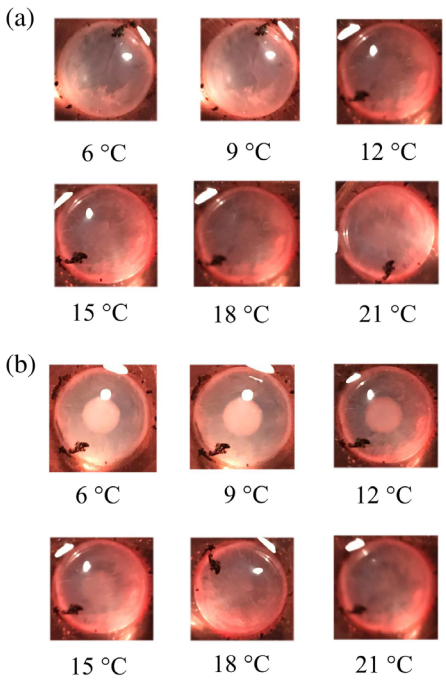

Fig. 3 (a) Images from a dissecting microscope while a fresh porcine lens was (a) cooled from 21°C to 6°C and (b) warmed from 6°C to 21°C after being in a 4°C refrigerator for 6 h. The scale bars are 1 mm.

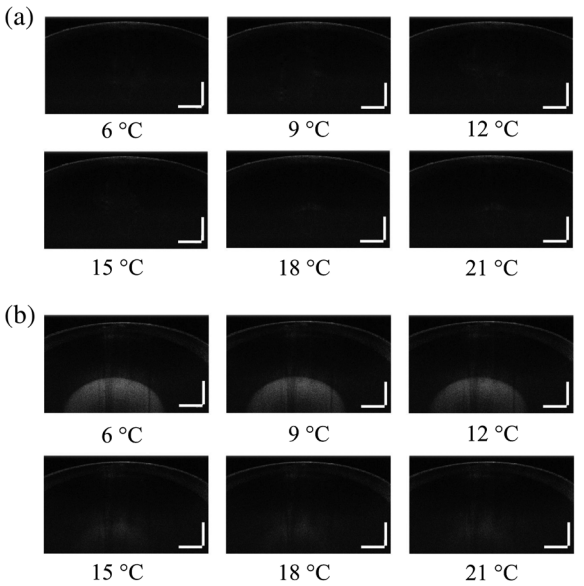

Fig. 4 (a) OCT structural images of a fresh porcine lens that was (a) cooled from 21°C to 6°C and (b) warmed from 6°C to 21°C after being in a 4°C refrigerator for 6 h. The scale bars are 1 mm.

transparency while the lens was cooled. However, after 6 h at 4°C, there is a clear opaque region in the center of the lens, which then disappeared as the lens was warmed to 21°C.

The OCT images corroborate these results. Figure 4 shows the OCT images of the lens before and after the formation of cold cataract. The OCT images of fresh lens did not show any scattering differences as a function of temperature while it was cooled. However, there was more scattering and a clear formation of aggregated scattering structures within the lens after cold cataract was formed. When the temperature was increased, the aggregated scattering structure shrank until it disappeared when the temperature increased beyond 12°C.

The relationship between stiffness and temperature before and after the cataract was formed is shown in Fig. 5. Figure 5(a) shows the elastic wave group velocity for one representative sample with and without cataract in the temperature range from 6°C to 21°C. Figure 5(b) shows the averaged elastic wave group velocities for all seven samples as a function of temperature. As seen in Figs. 3 and 4, the cataract began to disappear as the lens was warmed beyond 12°C. The group velocities in the samples that were cooled for 6 h at 4°C (cataract) decreased as they were warmed. Statistical testing by one-way ANOVA showed that there was no statistically significant difference of the group velocities for different temperatures in both cataract and normal groups [$F(5, 0.95) = 0.69$, $p = 0.64$]. A t-test showed that the difference in stiffness between cataract samples and normal samples was significant ($p = 0.003$). Based on this result, we performed further pairwise t-tests (with Bonferroni correction for multiple testing) for each temperature, which showed a significant difference between the stiffness of the cataract and normal lenses at 6°C, 9°C, and 12°C ($p = 0.012$, 0.007, and 0.0015, respectively). The values of Young's modulus of the lenses shown in Fig. 5(c) were calculated using Eq. (1). The mean value of the estimated Young's moduli of cataract lenses for 6°C, 9°C, 12°C was 21.8 ± 7.7 kPa, whereas the mean value of the Young's moduli of the normal lenses at this temperature was

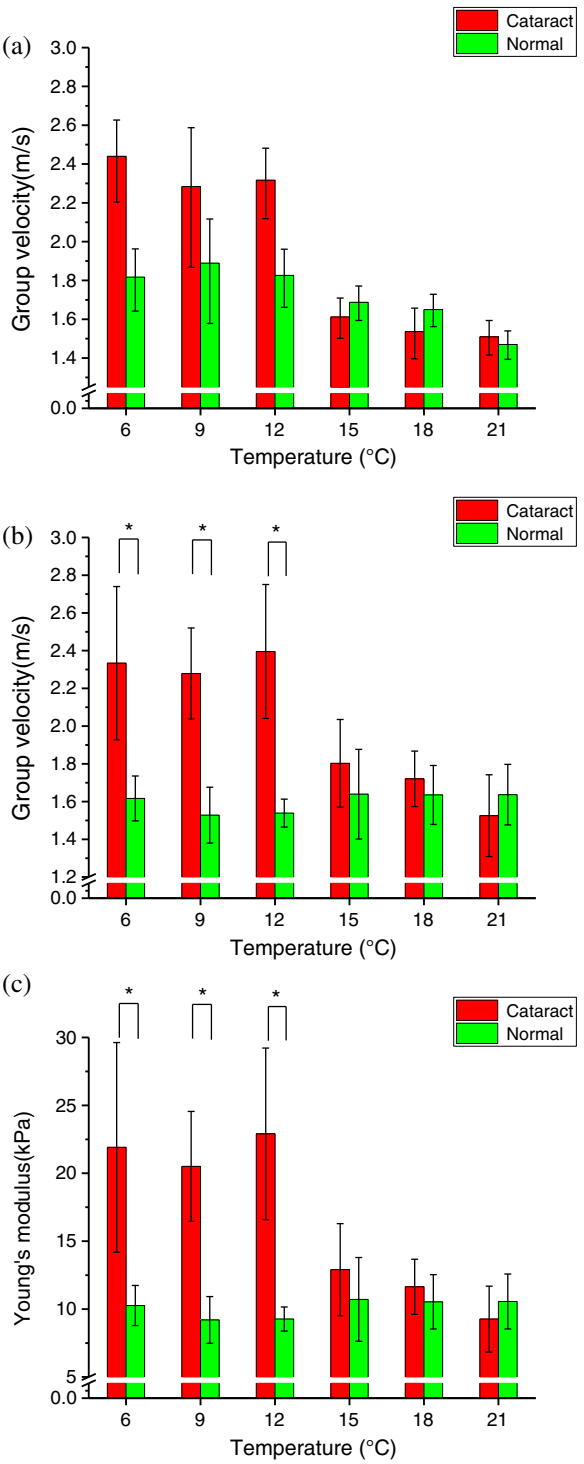

Fig. 5 The measured group velocities and estimated Young's moduli for the fresh lenses and lenses with induced cold cataracts. (a) The group velocity for the representative sample, in which the error bars represent the error estimated by the 95% confidence interval for the slope of a linear fit of the propagation time versus distance. (b) The averaged velocities and (c) Young's moduli for all samples ($n = 7$) where the error bars are the inter-sample standard deviation. The asterisks indicate statistical significance ($p < 0.05$) determined by student's t-test.

9.6 ± 1.4 kPa. For 15°C, 18°C, and 21°C, the cataract groups have the mean value of the Young's modulus of about 11.3 ± 3.4 kPa, and while the normal lenses groups have the mean value of the Young's moduli of 10.6 ± 2.3 kPa.

The measurements of the internal temperature gradient in cataract and normal lenses showed results similar to the results for the agar phantom, with no significant difference between normal and cataract lenses, within the measured temperatures range. For the normal lens, the mean difference between the internal temperature of the lens and the temperature of PBS solution was 0.43 ± 0.38°C, whereas for cataract lens, it was 0.42 ± 0.34°C. The maximum differences were 1.1°C and 1.0°C for normal and cataract lenses, respectively.

4 Discussion

While the relationship between the stiffness of the lens and the age is well known,[3,18,28,43] the influence of cataract formation on the lens stiffness is still unclear. In this work, we have demonstrated that in a porcine cold cataract model, the stiffness of the lens has a correlation with opacity of the nucleus. The speed of the elastic wave (i.e., stiffness of the lens) significantly decreased when cataract dissolved between 12°C and 15°C. Similar to the optical properties, the changes in lens stiffness are reversible, and possibly connected with the precipitation of γ-crystallin. Because the changes in lens opacity are localized in the nucleus, we could assume that the changes in lens elasticity are also localized in the nucleus, as it has been shown that there is an elastic gradient in the lens.[13,18] Although the OCE measurements were performed only on the lens surface, it is known that the surface wave is also sensitive to deep layers of the medium, depending on the wavelength of the elastic wave.[44–46] Though the scan width was greater than the width of the cold cataract, the width that we used to calculate group velocity was only ~3 mm across the center of the apex of the lens, which means the group velocity measurements were from the region over the cataract. In our case, as seen in Fig. 4, the cataract was located 2 to 3 mm below the surface of the lens. However, the frequency content of the elastic wave was below 1 kHz (centered around ~550 Hz). With a speed of ~1.8 m/s, the corresponding elastic wave wavelength was ~3.3 mm. Therefore, the estimated Young's modulus reflects some spatially averaged elastic modulus, including part of the nucleus, but likely underestimates the nucleus stiffness. Additional studies are required to better understand the spatial elasticity distribution in cataract lenses, and our future studies will be focused on a much wider range of elastic wave frequencies to probe the elasticity gradient of the lens.

Previous research shows that the threshold of the cold cataract might vary in different species.[7–9] Zigman and Lerman[5] demonstrated that the optical density of the mouse lens is stable up to 11°C. In our experiments on porcine lenses, the threshold was between 12°C and 15°C. The percentage of γ-crystallin in porcine nucleus is about 30%,[47] whereas the mouse nucleus contains 60% γ-crystallin.[48] The fish lens has 30.5% γ-crystallin, and the cataract temperature threshold was demonstrated to be about 5°C.[9,49] The relationship between γ-crystallin and cold cataract threshold needs to be further elucidated and is an avenue of future research. Although many biological tissues demonstrate the dependence of elasticity on temperature,[50–53] similar to the temperature dependence for gelatin phantoms shown in Fig. 2, we did not observe a significant change of the wave speed (i.e., stiffness) with temperature in fresh lenses (Fig. 5). Also, the cataract lenses were slightly softer than fresh lenses at 21°C as seen in Fig. 5. This observation can be associated with residual effects of cataract formation, or overall changes in lens elasticity after 6 h of storage, for example, the loss of crystalline proteins after storage.[54] Previous work has shown that the duration of heating can also increase the elasticity of the lens.[50] When human lenses were heated for 4 h, the shear modulus was ~4 kPa. When the heating time was increased to 8 h, the shear modulus increased to about ~7 kPa because of proteins denaturing at 50°C. In contrast, freezing porcine lenses at −80°C caused a decrease in the shear modulus from ~0.9 to ~0.3 kPa after 4 weeks. Nevertheless, there is little or no research focused on the changes in lenticular biomechanical properties due to moderately cold temperatures (near 4°C). We postulate that the aggregation of γ-crystallins formed during cold cataract contributes to an increase in lenticular stiffness. Further analysis is needed to confirm or disprove this hypothesis and is the focus of future work.

Although the difference in the spatial distribution of temperature in the lens could be a possible reason for the difference in stiffness between cataract and normal lenses, our measurements show that the temperature gradient in the normal and cataract lenses are similar, such that it is unlikely that the temperature distribution can be a reason for the difference in the elastic wave velocity. The temperature gradient in the agar phantom was greater but can be explained by the different thermal conductivity and the size of the agar phantom.

The values of Young's modulus obtained based on Eq. (1) are in agreement with literature data for porcine lenses.[12,55] However, the distribution of elasticity in crystalline lens is inhomogeneous.[17,43] In addition, viscous properties also could play a significant role in the process of surface wave propagation.[11,17,18] Therefore, application of Eq. (1) obtained for an elastic, homogeneous half-space has significant limitations. More sophisticated analytical and computational models are needed to provide more accurate values of lens viscoelasticity, which we are focused on developing.

5 Conclusion

In this work, we evaluated the changes in the biomechanical properties of porcine lenses *ex vivo* during the formation of cold cataract using OCE. The lenses with cold-induced cataracts showed an increase in elastic wave velocity, and correspondingly, stiffness, in comparison with fresh lenses. However, the difference in stiffness between cataract and fresh lenses disappeared after the cataract dissolved. These results show that OCE can assess lenticular biomechanical properties and may be useful for cataract characterization.

Disclosure

The authors have no relevant financial interests in this article and no potential conflicts of interest to disclose.

Acknowledgments

This work was supported by Grant No. R01EY022362 from the National Institutes of Health, Bethesda, Maryland.

References

1. D. Pascolini and S. P. Mariotti, "Global estimates of visual impairment: 2010," *Br. J. Ophthalmol.* **96**(5), 614–618 (2012).
2. B. Singh, D. Kumar, and R. Singh, "Phytotherapeutics for management and prevention of cataract generation," *Phytopharmacology* **3**(1), 93–110 (2012).
3. K. R. Heys and R. J. Truscott, "The stiffness of human cataract lenses is a function of both age and the type of cataract," *Exp. Eye Res.* **86**(4), 701–703 (2008).

4. R. J. Siezen et al., "Opacification of gamma-crystallin solutions from calf lens in relation to cold cataract formation," *Proc. Natl. Acad. Sci. U. S. A.* **82**(6), 1701–1705 (1985).
5. S. Zigman and S. Lerman, "Properties of a cold-precipitable protein fraction in the lens," *Exp. Eye Res.* **4**(1), 24–30 (1965).
6. S. Lerman and S. Zigman, "Metabolic studies on the cold precipitable protein of the lens," *Acta Ophthalmol.* **45**(2), 193–199 (1967).
7. T. Tanaka, C. Ishimoto, and L. T. Chylack Jr., "Phase separation of a protein-water mixture in cold cataract in the young rat lens," *Science* **197**(4307), 1010–1012 (1977).
8. J. G. Sivak, D. D. Stuart, and J. A. Weerheim, "Optical performance of the bovine lens before and after cold cataract," *Appl. Opt.* **31**(19), 3616–3620 (1992).
9. M. A. Loewenstein and F. A. Bettelheim, "Cold cataract formation in fish lenses," *Exp. Eye Res.* **28**(6), 651–663 (1979).
10. A. Banh and J. G. Sivak, "Laser scanning analysis of cold cataract in young and old bovine lenses," *Mol. Vision* **10**, 144–147 (2004).
11. H. A. Weeber et al., "Dynamic mechanical properties of human lenses," *Exp. Eye Res.* **80**(3), 425–434 (2005).
12. S. Krag and T. T. Andreassen, "Biomechanical measurements of the porcine lens capsule," *Exp. Eye Res.* **62**(3), 253–260 (1996).
13. T. N. Erpelding, K. W. Hollman, and M. O'Donnell, "Mapping age-related elasticity changes in porcine lenses using bubble-based acoustic radiation force," *Exp. Eye Res.* **84**(2), 332–341 (2007).
14. H. A. Weeber and R. G. L. van der Heijde, "On the relationship between lens stiffness and accommodative amplitude," *Exp. Eye Res.* **85**(5), 602–607 (2007).
15. H. J. Burd, G. S. Wilde, and S. J. Judge, "An improved spinning lens test to determine the stiffness of the human lens," *Exp. Eye Res.* **92**(1), 28–39 (2011).
16. S. Yoon et al., "The mechanical properties of ex vivo bovine and porcine crystalline lenses: age-related changes and location-dependent variations," *Ultrasound Med. Biol.* **39**(6), 1120–1127 (2013).
17. K. W. Hollman, M. O'Donnell, and T. N. Erpelding, "Mapping elasticity in human lenses using bubble-based acoustic radiation force," *Exp. Eye Res.* **85**(6), 890–893 (2007).
18. S. Yoon et al., "A high pulse repetition frequency ultrasound system for the ex vivo measurement of mechanical properties of crystalline lenses with laser-induced microbubbles interrogated by acoustic radiation force," *Phys. Med. Biol.* **57**(15), 4871–4884 (2012).
19. M. R. Hee et al., "Optical coherence tomography of the human retina," *Arch Ophthalmol.* **113**(3), 325–332 (1995).
20. D. Huang et al., "Optical coherence tomography," *Science* **254**(5035), 1178–1181 (1991).
21. K. V. Larin and D. D. Sampson, "Optical coherence elastography—OCT at work in tissue biomechanics [Invited]," *Biomed. Opt. Express* **8**(2), 1172–1202 (2017).
22. J. Schmitt, "OCT elastography: imaging microscopic deformation and strain of tissue," *Opt. Express* **3**(6), 199–211 (1998).
23. M. Sticker et al., "Quantitative differential phase measurement and imaging in transparent and turbid media by optical coherence tomography," *Opt. Lett.* **26**(8), 518–520 (2001).
24. M. A. Kirby et al., "Optical coherence elastography in ophthalmology," *J. Biomed. Opt.* **22**(12), 121720 (2017).
25. S. Park et al., "The impact of intraocular pressure on elastic wave velocity estimates in the crystalline lens," *Phys. Med. Biol.* **62**(3), N45–N57 (2017).
26. R. Manapuram et al., "Assessment of wave propagation on surfaces of crystalline lens with phase sensitive optical coherence tomography," *Laser Phys. Lett.* **8**(2), 164–168 (2010).
27. S. Wang et al., "Assessing the mechanical properties of tissue-mimicking phantoms at different depths as an approach to measure biomechanical gradient of crystalline lens," *Biomed. Opt. Express* **4**(12), 2769–2780 (2013).
28. C. Wu et al., "Assessing age-related changes in the biomechanical properties of rabbit lens using a coaligned ultrasound and optical coherence elastography system," *Invest. Ophthalmol. Visual Sci.* **56**(2), 1292–1300 (2015).
29. C. Wu et al., "Assessing the biomechanical properties of the porcine crystalline lens as a function of intraocular pressure with optical coherence elastography," *Biomed. Opt. Express* **9**(12), 6455–6466 (2018).
30. A. P. Sarvazyan et al., "Shear wave elasticity imaging: a new ultrasonic technology of medical diagnostics," *Ultrasound Med. Biol.* **24**(9), 1419–1435 (1998).
31. E. T. Detorakis et al., "Evaluation of iridociliary and lenticular elasticity using shear-wave elastography in rabbit eyes," *Acta Med.* (Hradec Kralove) **57**(1), 9–14 (2014).
32. X. Zhang et al., "Noninvasive assessment of age-related stiffness of crystalline lenses in a rabbit model using ultrasound elastography," *Biomed. Eng. Online* **17**(1), 75 (2018).
33. E. F. Carbajal et al., "Revealing retroperitoneal liposarcoma morphology using optical coherence tomography," *J. Biomed. Opt.* **16**(2), 020502 (2011).
34. S. Wang et al., "A focused air-pulse system for optical-coherence-tomography-based measurements of tissue elasticity," *Laser Phys. Lett.* **10**(7), 75605 (2013).
35. S. Wang and K. V. Larin, "Shear wave imaging optical coherence tomography (SWI-OCT) for ocular tissue biomechanics," *Opt. Lett.* **39**(1), 41–44 (2014).
36. M. Singh et al., "Applicability, usability, and limitations of murine embryonic imaging with optical coherence tomography and optical projection tomography," *Biomed. Opt. Express* **7**(6), 2295–2310 (2016).
37. J. Li et al., "Dynamic optical coherence tomography measurements of elastic wave propagation in tissue-mimicking phantoms and mouse cornea in vivo," *J. Biomed. Opt.* **18**(12), 121503 (2013).
38. S. Song, Z. Huang, and R. K. Wang, "Tracking mechanical wave propagation within tissue using phase-sensitive optical coherence tomography: motion artifact and its compensation," *J. Biomed. Opt.* **18**(12), 121505 (2013).
39. Z. Han et al., "Quantitative methods for reconstructing tissue biomechanical properties in optical coherence elastography: a comparison study," *Phys. Med. Biol.* **60**(9), 3531–3547 (2015).
40. J. F. Doyle, *Wave Propagation in Structure: Spectral Analysis Using Fast Discrete Fourier Transforms*, Mechanical Engineering Series, Springer, New York (1997).
41. A. S. Vilupuru and A. Glasser, "Optical and biometric relationships of the isolated pig crystalline lens," *Ophthalmic Physiol. Opt.* **21**(4), 296–311 (2001).
42. R. F. Fisher, "The elastic constants of the human lens," *J. Physiol.* **212**(1), 147–180 (1971).
43. H. A. Weeber et al., "Stiffness gradient in the crystalline lens," *Graefes Arch. Clin. Exp. Ophthalmol.* **245**(9), 1357–1366 (2007).
44. S. R. Aglyamov et al., "The dynamic deformation of a layered viscoelastic medium under surface excitation," *Phys. Med. Biol.* **60**(11), 4295–4312 (2015).
45. K. D. Mohan and A. L. Oldenburg, "Elastography of soft materials and tissues by holographic imaging of surface acoustic waves," *Opt. Express* **20**(17), 18887–18897 (2012).
46. E. Soczkiewicz, "The penetration depth of Rayleigh surface waves," *Acustica* **82**(2), 380–382 (1996).
47. J. Keenan, D. F. Orr, and B. K. Pierscionek, "Patterns of crystallin distribution in porcine eye lenses," *Mol. Vision* **14**, 1245–1253 (2008).
48. S. Lerman, S. Zigman, and W. F. Forbes, "Properties of a cryoprotein in the ocular lens," *Biochem. Biophys. Res. Commun.* **22**(1), 57–61 (1966).
49. M. Posner et al., "A proteome map of the zebrafish (Danio rerio) lens reveals similarities between zebrafish and mammalian crystallin expression," *Mol. Vision* **14**, 806–814 (2008).
50. K. R. Heys, M. G. Friedrich, and R. J. Truscott, "Presbyopia and heat: changes associated with aging of the human lens suggest a functional role for the small heat shock protein, α-crystallin, in maintaining lens flexibility," *Aging Cell* **6**(6), 807–815 (2007).
51. M. N. Miranda, "Environmental temperature and senile cataract," *Trans. Am. Ophthalmol. Soc.* **78**, 255–264 (1980).
52. E. Asmussen, F. Bonde-Petersen, and K. Jørgensen, "Mechano-elastic properties of human muscles at different temperatures," *Acta Physiol. Scand.* **96**(1), 83–93 (1976).
53. S. M. Elmore et al., "Nature of 'imperfect' elasticity of articular cartilage," *J. Appl. Physiol.* **18**(2), 393–396 (1963).
54. S. Reiß et al., "Ex vivo measurement of postmortem tissue changes in the crystalline lens by Brillouin spectroscopy and confocal reflectance microscopy," *IEEE Trans. Biomed. Eng.* **59**(8), 2348–2354 (2012).

55. P.-H. Tsui et al., "Feasibility study of using high-frequency ultrasonic Nakagami imaging for characterizing the cataract lens in vitro," *Phys. Med. Biol.* **52**(21), 6413–6425 (2007).

Hongqiu Zhang is a PhD student of biomedical engineering at the University of Houston. He is studying optical coherence tomography in Dr. Kirill V. Larin's lab. Currently, he is working on elastography based on OCT and the combination of OCT/OPT and SPIM. He works on crystalline lens and other ophthalmological tissues. His research interests include elastography imaging of medicine and its after effects of the biological tissue.

Chen Wu received his BS degree in optical information science and technology from Ocean University of China in 2010, MS degree in biomedical engineering from Martin Luther University Halle-Wittenberg in Germany in 2013, and PhD from the Department of Biomedical Engineering at the University of Houston in 2018. His research interests are in the development of optical coherence tomography technique and the application in different biomedical fields, such as embryonic imaging, ophthalmology, and tissue biomechanics.

Manmohan Singh is current a postdoctoral fellow in Dr. Kirill Larin's Biomedical Optics Laboratory at the University of Houston. He received his PhD in biomedical engineering from the University of Houston in 2018. His research interests are focused on developing optical elastography modalities and image processing techniques to noninvasively detect diseases.

Achuth Nair is a PhD candidate at the University of Houston Biomedical Optics Laboratory under the supervision of Dr. Kirill Larin. He received his bachelor's degree in biomedical engineering at the University of Houston and stayed on to continue his graduate studies. His research interests include using optical coherence elastography to analyze tissue biomechanical properties to characterize tissue health.

Salavat R. Aglyamov received his BS and MS degrees in applied mathematics in 1991 and 1993, respectively, from Moscow State University, Moscow, Russia. He received his PhD in biophysics from the Institute of Theoretical and Experimental Biophysics, Russia, in 1999. Currently, he is a research assistant professor in the Department of Mechanical Engineering at the University of Houston. His research interests are in the areas of tissue biomechanics, elastography, applied mathematics, ultrasound, OCT, and photoacoustics.

Kirill V. Larin is a professor of Biomedical Engineering at the University of Houston. He received his MS degree in laser physics and mathematics from the Saratov State University in 1995, PhD in biomedical engineering from the University of Texas Medical Branch in Galveston in 2002. He has published more than 100 papers in the field of biomedical optics and biophotonics. He was inducted as fellow of SPIE in 2015 and OSA in 2016.